4816 *Biochemistry* **2009,** *48,* 4816–4827
DOI: 10.1021/bi9002265

BIOCHEMISTRY
including biophysical chemistry & molecular biology
Article

Effects of pH and Iminosugar Pharmacological Chaperones on Lysosomal Glycosidase Structure and Stability[†,‡]

Raquel L. Lieberman,*[,§,∥,⊥] J. Alejandro D'aquino,[∥] Dagmar Ringe,[∥] and Gregory A. Petsko[§,∥]

[§]*Structural Neurology Lab at the Center for Neurologic Diseases, Brigham and Women's Hospital and Harvard Medical School, 77 Avenue Louis Pasteur, Boston, Massachusetts 02115, and* [∥]*Rosenstiel Basic Biomedical Sciences Research Center, Brandeis University, 415 South Street, Waltham, Massachusetts 02454* [⊥]*Current address: School of Chemistry and Biochemistry and Institute of Bioengineering and Biosciences, Georgia Institute of Technology, 901 Atlantic Dr. NW, Atlanta, GA 30318*

Received February 10, 2009; Revised Manuscript Received April 6, 2009

ABSTRACT: Human lysosomal enzymes acid-β-glucosidase (GCase) and acid-α-galactosidase (α-Gal A) hydrolyze the sphingolipids glucosyl- and globotriaosylceramide, respectively, and mutations in these enzymes lead to the lipid metabolism disorders Gaucher and Fabry disease, respectively. We have investigated the structure and stability of GCase and α-Gal A in a neutral-pH environment reflective of the endoplasmic reticulum and an acidic-pH environment reflective of the lysosome. These details are important for the development of pharmacological chaperone therapy for Gaucher and Fabry disease, in which small molecules bind mutant enzymes in the ER to enable the mutant enzyme to meet quality control requirements for lysosomal trafficking. We report crystal structures of apo GCase at pH 4.5, at pH 5.5, and in complex with the pharmacological chaperone isofagomine (IFG) at pH 7.5. We also present thermostability analysis of GCase at pH 7.4 and 5.2 using differential scanning calorimetry. We compare our results with analogous experiments using α-Gal A and the chaperone 1-deoxygalactonijirimycin (DGJ), including the first structure of α-Gal A with DGJ. Both GCase and α-Gal A are more stable at lysosomal pH with and without their respective iminosugars bound, and notably, the stability of the GCase−IFG complex is pH sensitive. We show that the conformations of the active site loops in GCase are sensitive to ligand binding but not pH, whereas analogous galactose- or DGJ-dependent conformational changes in α-Gal A are not seen. Thermodynamic parameters obtained from α-Gal A unfolding indicate two-state, van't Hoff unfolding in the absence of the iminosugar at neutral and lysosomal pH, and non-two-state unfolding in the presence of DGJ. Taken together, these results provide insight into how GCase and α-Gal A are thermodynamically stabilized by iminosugars and suggest strategies for the development of new pharmacological chaperones for lysosomal storage disorders.

Glycoside hydrolases are involved in turnover of intracellular substrates in an acidic environment [pH ∼5.2 (*1*)] of the lysosome. These enzymes are synthesized and folded in the neutral-pH environment of the endoplasmic reticulum (ER),[1] exported to the Golgi apparatus for sorting, and subsequently trafficked to lysosomes. Inherited genetic mutations in specific glycoside hydrolases result in enzyme deficiency in the lysosome and the family of diseases called lysosomal storage disorders, including Anderson-Fabry, Gaucher, Tay-Sachs, and Sandhoff diseases (*2*, *3*). Many of the mutations associated with these diseases are missense mutations that result in single-amino acid substitutions remote from the active site of these enzymes, however. Such

[†]This work was supported by National Institutes of Health (NIH) Fellowship F32AG027647 to R.L.L., as well as the McKnight Endowment for Neuroscience (D.R. and G.A.P.). The Biophysical Instrumentation Facility for the Study of Complex Macromolecular Systems at the Massachusetts Institute of Technology is funded by National Science Foundation Grant NSF-0070319 and NIH Grant GM68762. The Advanced Photon Source was supported by the U.S. Department of Energy, Basic Energy Sciences, Office of Science, under Contract W-31-109-ENG-38. GM/CA CAT has been funded in whole or in part with federal funds from the National Cancer Institute (Y1-CO-1020) and the National Institute of General Medical Science (Y1-GM-1104). BioCARS Sector 14 was supported by the National Institutes of Health, National Center for Research Resources, under Grant RR007707.

[‡]Protein Data Bank entries 3GXF (C1), 3GXI (C2), 3GXM (C3), 3GXD (C4), 3GXN (L1), 3GXP (L2), and 3GXT (L3).

*To whom correspondence should be addressed. Phone: (404) 385-3663. Fax: (404) 294-2295. E-mail: raquel.lieberman@chemistry.gatech.edu.

[1]Abbreviations: GCase, acid-β-glucosidase; α-Gal A, acid-α-galactosidase; IFG, isofagomine; DGJ, 1-deoxygalactonijirimycin; ER, endoplasmic reticulum; ERT, enzyme replacement therapy; FDA, Food and Drug Administration; SRT, substrate reduction therapy; LSDs, lysosomal storage disorders; TIM, triosephosphate isomerase; SSM, secondary structure matching; DSC, differential scanning calorimetry; T_m, melting temperature; ΔH_{cal}, calorimetric enthalpy; ΔH_{vH}, van't Hoff enthalpy; IC_{50}, half-inhibitory concentration; ERAF, ER-assisted folding; ERAD, ER-associated degradation; LIMP-2, lysosomal integral membrane II; PDB, Protein Data Bank; rmsd, root-mean-square deviation.

Published on Web 04/20/2009

mutant enzymes retain at least partial catalytic activity in vitro (*4*, *5*) but exhibit impaired cellular trafficking (*6*−*8*). Only correctly folded proteins in the ER are efficiently transported to the Golgi apparatus and then to their intended cellular destinations. Aberrantly folded molecules are recognized by the ER quality control system and are either retained in this compartment, sent out of the ER for proteolytic degradation via the proteasome, or a combination thereof (*9*, *10*). Thus, pathophysiology in lysosomal storage disorders is not linked directly to abolished intrinsic enzyme activity, but first to a defect in protein stability, then to a defect in cellular trafficking, and finally to reduced lysosomal hydrolase activity (*6*−*8*). The mutant protein accumulates in either the ER, the Golgi, or endocytic vesicles and is then targeted for degradation, and a reduced level of active enzyme reaches the lysosome (*7*).

The current standard of care for individuals with lysosomal storage diseases is enzyme replacement therapy (ERT) (*11*, *12*), in which an intravenous infusion of recombinant wild-type human enzyme is internalized by affected cells via cell surface receptors and delivered to lysosomes to break down accumulated substrate. Another FDA-approved treatment approach for certain types of Gaucher disease, called substrate reduction therapy (SRT), utilizes a small molecule inhibitor of glycolipid synthesis to reduce substrate production (*13*, *14*). These treatments address substrate accumulation but do not address the protein folding defects and their potential contributions such as release of pro-inflammatory cytokines (*15*) that may play a role in the pathophysiology of these diseases.

Pharmacological chaperones constitute a promising new treatment strategy for diseases of protein misfolding and mistrafficking, and compounds are currently being evaluated for lyososomal storage disorders (LSDs) (*3*, *16*−*19*), among others (*20*). In this approach, a tailored small molecule inhibitor of a target lysosomal enzyme binds to the protein during initial biosynthesis and folding in the ER. Different competitive inhibitors are in development as candidate chaperones for various LSDs (*7*, *21*−*33*). Although somewhat counterintuitive, enzyme inhibitors can increase steady-state lysosomal levels of active enzymes by enabling the mutant protein to meet quality control standards in the ER and restore trafficking (*34*).

The mechanism by which pharmacological chaperones function is not known, but two scenarios can be envisioned. The structure of a folded mutant enzyme that retains partial catalytic activity is likely to be very similar to the native, wild-type structure. Thus, pharmacological chaperones might bind to a fully folded mutant protein target to stabilize a nativelike conformation. Alternatively, mutations may affect the folding pathway by stabilizing a non-native, less stable intermediate state. In this case, the pharmacological chaperone may bind to a non-native conformation and accelerate the transition to the nativelike state. Once in the final subcellular destination and in the presence of substrate, the inhibitor dissociates from the mutant enzyme, and the enzyme can then perform its function. Clinically, the dissociation of the inhibitor can be optimized through the dosing regimen, which can be tailored to the cellular lifetime of the enzyme of interest. For example, lysosomal hydrolases have half-lives on the order of a few days (*35*).

In this paper, we have characterized the effects of pH and pharmacological chaperone binding on the structure and thermostability of acid-α-galactosidase (α-Gal A) and acid-β-glucosidase (GCase), enzymes whose mutations lead to the lysosomal storage disorders Anderson-Fabry (*12*) and Gaucher disease (*36*, *37*), respectively. Despite exhibiting a very low level of sequence similarity, the three-dimensional structures of GCase [EC 3.2.1.45, CaZY (*38*) glycoside hydrolase family 30, ∼60 kDa monomer] (*23*, *39*) and α-Gal A (EC 3.2.1.22, CaZY glycoside hydrolase family 27, ∼50 kDa monomer) (*40*) (Figure 1) share a TIM barrel [$(\alpha/\beta)_8$] motif in the catalytic domain and an immunoglobulin fold in the same relative position (overall rmsd for Cα atoms of ∼4.5 Å). In α-Gal A, the ∼300 N-terminal residues comprise the TIM barrel and the ∼100 C-terminal residues make up the predominantly β-sheet-containing immunoglobulin-like domain (*40*) (Figure 1a). In the larger enzyme, GCase, the connectivity between participating elements of secondary structure is different from that of α-Gal A. Each tertiary structural element in GCase is composed of contributions from disparate regions of the sequence, and the additional three-stranded β-sheet brings together in space, and stabilizes, the N- and C-terminal ends (*39*) (Figure 1b). Whereas α-Gal A is a dimer (*40*−*44*), the oligomeric state of GCase has been shown to be a monomer when isolated from normal spleens (*45*−*47*) but a dimer when isolated from Gaucher patients (*45*, *47*). Both enzymes retain the stereochemistry of their respective substrate and product, and the catalytic nucleophile and proton donor are either two aspartate residues (α-Gal A) (*40*, *48*) or two glutamate residues (GCase) (*4*, *49*). Finally, both enzymes are activated by saposins. Globosyltriosylceramide, the substrate for α-Gal A involved in Fabry disease, binds saposin B prior to presentation to α-Gal A (*50*). Compared to globotriosylceramide, the substrate for GCase, glucosylceramide, is considerably more hydrophobic, yet glucosylceramide is hydrolyzed by GCase directly without the need for the activator. GCase activity is enhanced by saposin C, however (*51*, *52*).

Recently, we demonstrated that the potent iminosugar inhibitor isofagomine (IFG) acts as a pharmacological chaperone by improving protein trafficking for the N370S mutant GCase enzyme, resulting in increased cellular GCase levels in patient-derived fibroblasts (*23*). The structure of IFG-bound GCase at pH 4.5 (Figure 1b, PDB entry 2NSX) revealed a substantial rearrangement of one region (loop 1, residues 311−319) from an extended loop to an α-helical conformation, at the mouth of the active site. This induced fit has several important ramifications. First, a new surface topology is created, including two hydrophobic grooves extending from the site of catalysis in the triosephosphate isomerate (TIM) barrel domain. Second, these hydrophobic surfaces are suitable for binding of the alkyl chains of glucosylceramide. Third, Asn 370, located on the interior of GCase on a stable helix and the most common mutation site that causes type 1 Gaucher disease, plays a direct role in stabilizing the configuration of loop 1 in the new conformation. Lastly, Tyr 313, located on loop 1, both stabilizes loop 1 in the α-helical conformation and alters its H-bonding pattern between the proton donor and catalytic nucleophile in the active site. We now extend our investigations to include a comparison of GCase structures at different pHs to elucidate the details of the active site loop conformations and stability conferred by inhibitor binding. Interestingly, analogous studies of α-Gal A with the pharmacological chaperone deoxygalactonijirimycin (DGJ) (*16*, *22*, *53*−*55*) do not reveal major conformational changes upon pH, inhibitor, or product binding, suggesting that, unlike GCase, α-Gal A may bind its subtrate like a "lock and key". Taken together, our data support the model of pharmacological chaperoning in which the inhibitor binds to and stabilizes the nativelike state of the target enzyme.

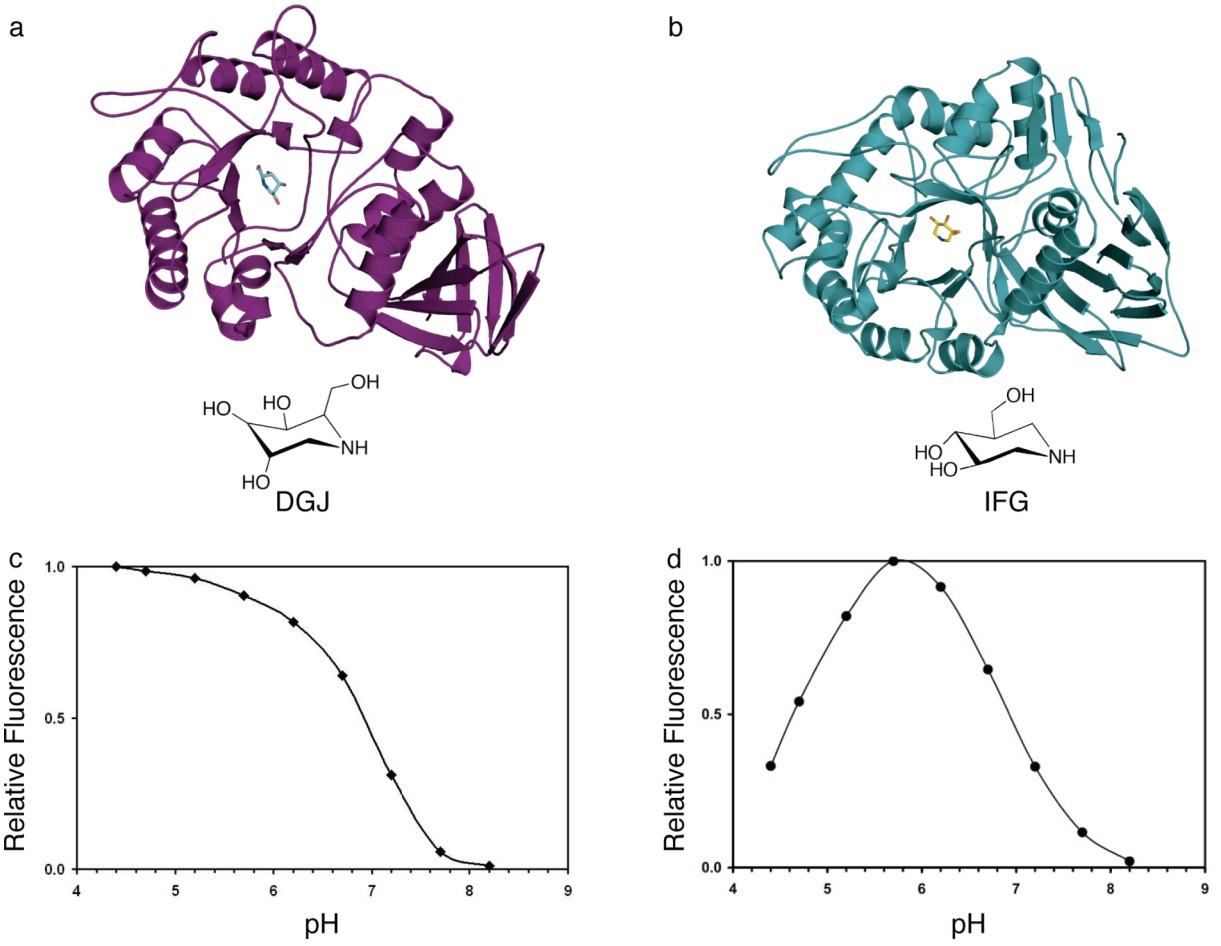

FIGURE 1: Cartoon representation of (a) α-Gal A with DGJ (this work) and (b) GCase with IFG (PDB entry 2NSX). DGJ and IFG are pictured as ball-and-stick diagrams, and their chemical structures are depicted below their respective cartoons. (c) Activity profile of α-Gal A as a function of pH and (d) activity profile of GCase as a function of pH.

EXPERIMENTAL PROCEDURES

Crystallization, Data Collection, Structure Determination, and Refinement. We purchased lyophilized, recombinant human acid-β-glucosidase (Cerezyme) and acid-α-galactosidase (Fabrazyme, both Genzyme Corp.) from Brigham and Women's Hospital pharmacy. We reconstituted Cerezyme and Fabrazyme with phosphate-buffered saline (Sigma) to ~1 mg/mL and partially deglycosylated the enzymes for 3 days using N-glycosidase F (Glyko, Novato, CA) as described previously (*39*). The deglycosylation step improves crystal quality but does not affect protein structure (*56*). We determined crystal structures of IFG-bound GCase at pH 7.5 (C1), apo GCase at pH 5.5 (C2), two structures of apo GCase at pH 4.5 (C3 and C4), and apo α-Gal A (L1), galactose-bound α-Gal A (L2), and DGJ-bound α-Gal A at pH 7.5 (L3). A summary of conditions appears in Table 1.

GCase was crystallized by hanging drop vapor diffusion, similar to methods reported previously, with some modification described below. GCase crystals at pH 4.5 (C3) were grown by hanging drop vapor diffusion using a cocktail containing 1 M ammonium sulfate, 0.1 M acetate buffer (pH 4.5), 0.17 M guanidinium hydrochloride, and 0.02 M KCl (*39*). The crystals were then harvested in a solution of 0.1 M acetate buffer (pH 4.5) and 1.8 M Li_2SO_4 just prior to being flash-cooled in liquid nitrogen. GCase crystals at pH 4.5 (C4) were obtained by soaking C2 crystals, which were grown by vapor diffusion over a solution containing 0.8 M NaH_2PO_4, 0.8 M KH_2PO_4, and 0.1 M citrate buffer (pH 5.5), for 10 min in a solution containing 0.1 M acetate buffer (pH 4.5) and 1.8 M Li_2SO_4. Both C2 and C3 crystals were then flash-cooled in liquid nitrogen. The C1 crystals were obtained by soaking GCase crystals grown at pH 7.5 (*23*) in mother liquor containing 500 μM IFG for 10 min. C1 crystals were cryoprotected with mother liquor and 20% glycerol.

α-Gal A was crystallized as described previously (*40*) with some modifications. After deglycosylation, we exchanged α-Gal A into 20 mM Tris (pH 7.5) using concentration devices with a molecular mass cutoff of 10000 kDa (Millipore). Crystallization trials were conducted with 10, 20, and 40 mg/mL deglycosylated α-Gal A. Independent of the protein concentration, crystals grew using hanging drop vapor diffusion from a cocktail containing 0.1 M acetate buffer (pH 4.5), 20−25% PEG 4000, and 0.15−0.22 M ammonium sulfate. Crystals appeared after 1 week (40 mg/mL) or after 2 months (10 mg/mL) and ranged in size from 0.05 mm × 0.05 mm × 0.1 mm (40 mg/mL) to 0.4 mm × 0.4 mm × 1 mm (10 or 20 mg/mL). Crystals were soaked for 1 h with 200 μM DGJ (L3) in mother liquor or 0.1 M galactose (L2) in mother liquor. Prior to cooling, crystals were transferred to a solution containing mother liquor (no DGJ, no galactose) supplemented with 30% ethylene glycol. Apo α-Gal A (L1) crystals were flash-cooled after cryoprotection with paratone-n.

Crystallographic data were collected at the GM/CA-CAT (C1, C2, C4, and L1−L3) and Bio-CARS (C3) beamlines at the Advanced Photon Source (Darien, IL) and processed with

Table 1: Summary of Structures and Their Roles in This Investigation

crystal	crystallization condition	role in investigation	PDB entry
C1	Na/KH_2PO_4, Hepes (pH 7.5) soak: IFG cryo: glycerol	pH dependence of IFG binding on GCase structure	3GXF
C2	Na/KH_2PO_4, citrate buffer (pH 5.5) cryo: Li_2SO_4	apo GCase structure at high limit of lysosomal pH	3GXI
C3	$(NH_4)_2(SO_4)$, acetate buffer (pH 4.5), guanidinium hydrochloride, KCl cryo: Li_2SO_4	apo GCase structure at low limit of lysosomal pH and effect of crystallization cocktail (compare to C4)	3GXM
C4	same as C2 soak: acetate buffer (pH 4.5) cryo: Li_2SO_4	apo structure at low limit of lysosomal pH and effect of crystallization cocktail (compare to C3)	3GXD
L1	acetate buffer (pH 4.5), PEG 4000, ammonium sulfate cryo: paratone-n	apo α-Gal A, lysosomal pH	3GXN
L2	acetate buffer (pH 4.5), PEG 4000, ammonium sulfate soak: galactose cryo: ethylene glycol	galactose-bound α-Gal A, lysosomal pH	3GXP
L3	acetate buffer (pH 4.5), PEG 4000, ammonium sulfate soak: DGJ cryo: ethylene glycol	DGJ-bound α-Gal A, lysosomal pH	3GXT

XDS (*57*) (L3) or HKL2000 (*58*) (C1−C4, L1, and L2). The structures of GCase were determined by rigid body refinement in Refmac5 (*59*) using a protein model derived from PDB entry 2NT0 after deletion of loop 1 (residues 312−319) and loop 2 (residues 342−350) from all four copies in the asymmetric unit, as well as all N-linked carbohydrates, phosphate anions, and waters. The structures of α-Gal A were determined by molecular replacement with Molrep (*59*) using a monomeric search model derived from PDB entry 1R46 (*40*). We fit the atomic models into their respective electron density maps using Coot (*60*) and refined them using Refmac5 (*59*). We used medium noncrystallographic symmetry restraints for α-Gal A structures, generated topology and geometry restraints for IFG and DGJ using PRODRG2 (*61*), and identified bound water molecules using Coot (*60*). The percentage of residues in the most favored and additional allowed regions of the Ramachandran plot is 99.4−100% for all data sets, and crystallographic statistics are listed in Table 2. The Secondary Structure Matching (SSM) algorithm (*62*) from Coot was used for superposition, and figures were generated using Pymol (DeLano Scientific, San Carlo, CA).

Differential Scanning Calorimetry (DSC). Scanning calorimetric experiments were performed with a VP-DSC (Microcal Inc., Northampton, MA) microcalorimeter. Samples of lyophilized α-Gal A (Fabrazyme) and GCase (Cerezyme) were reconstituted in the appropriate buffer and dialyzed for 6−16 h using a Slide-a-lyzer (Pierce, 10000 kDa molecular mass cutoff) and degassed prior to the experiment. For α-Gal A (~50 μM), thermal denaturation curves were measured at pH 7.5 using phosphate-buffered saline (10 mM phosphate, 0.0027 M KCl, and 0.138 M NaCl) (Sigma) and at pH 5.2 using 10 mM acetate, 0.0027 M KCl, and 0.138 M NaCl. Buffers used for GCase (~25 μM) included 30 mM phosphate and 0.15 M NaCl (pH 7.5) or 30 mM acetate and 0.15 M NaCl (pH 5.15). For inhibitor studies, GCase or α-Gal A was incubated with 0.05−2.5 mM IFG or 0.05−3.8 mM DGJ at room temperature, respectively. All samples were prepared and measured in duplicate or triplicate.

To study the concentration dependence of the melting temperature, we recorded DSC thermograms at 47.5 and 8.6 μM for α-Gal A and 25, 9.6, or 14 μM for GCase. We observed no concentration-dependent change in melting temperature (T_m) for either apo α-Gal A or apo GCase (data not shown), suggesting that neither protein undergoes a classic dissociation mechanism upon unfolding under the experimental conditions. Thermal denaturation curves for for GCase were irreversible due to precipitation at high temperatures and could not be analyzed using equilibrium thermodynamics. To determine conditions for microscopic reversibility of unfolding for α-Gal A, we analyzed the scan rate dependence of the thermograms. We saw no difference between melting temperatures obtained by scans measured with rates of 1 and 1.5 °C/min, and all subsequent scans were measured at a rate of 1 °C/min. Thus, we were able to apply equilibrium thermodynamics analysis to the α-Gal A system.

DSC data were analyzed with Microcal Origin 7. Scans were first corrected by subtracting the sample trace from that of the buffer alone, and the concentrations were normalized (*63*). In the case of GCase, severe aggregation upon melting precluded further fitting to a thermodynamic model. As a measure of protein stability, our analysis is limited to differences in the T_m of the normalized data. For α-Gal A, data were fit to a non-two-state model, which provides the calorimetric (ΔH_{cal}) and van't Hoff (ΔH_{vH}) enthalpies. ΔH_{cal} is the measured enthalpy during protein unfolding, whereas ΔH_{vH} is the theoretical enthalphy of the transition assuming a two-state model. The cooperativity unit is defined by the ratio $\Delta H_{cal}/\Delta H_{vH}$. Sturtevant analysis was conducted as described previously (*64*−*66*).

Enzyme Activity Assays. The results of enzyme activity assays were kindly provided by Amicus Therapeutics. In brief, enzymatic activities of α-Gal A or GCase [50 ng prepared in 0.1 M citrate and 0.2 M phosphate buffer (pH 5.2) containing 0.1% Triton X-100 and 0.25% sodium taurocholate] were determined by incubating the enzymes in the presence of 3 mM 4-methylumbelliferyl-α-D-galactopyranoside or 4-methylumbelliferyl-β-D-glucopyranoside, respectively, in reaction buffer (50 mM sodium phosphate and 150 mM sodium chloride) adjusted to pH 4.4−8.2. After incubation at 37 °C for 1 h, the reactions were stopped by the addition of an equal volume of 0.5 M sodium carbonate (pH 10.8). The fluorescence of liberated substrate was read on a plate reader (excitation at 355 nm,

Table 2: Data Collection and Refinement Statistics

	GCase−IFG, pH 7.5 (C1)	GCase, pH 5.5 (C2)	GCase, pH 4.5 (C3)	GCase, pH 4.5, soaked (C4)	α-Gal A (L1)	α-Gal A−Gal (L2)	α-Gal A−DGJ (L3)
Data Collection							
space group	$P2_1$	$P2_1$	$P2_1$	$P2_1$	$P3_221$	$P3_221$	$P3_221$
cell dimensions							
a, *b*, *c* (Å)	110.3, 92.0, 152.4	110.05, 91.7, 152.3	110.5, 91.8, 152.8	109.3, 91.7, 152.5	90.4, 90.4, 217.5	89.5, 89.5, 215.9	89.6, 89.6, 216.6
α, *β*, *γ* (deg)	90, 111.2, 90	90, 111.1, 90	90, 111.2, 90	90, 111.0, 90	90, 90, 120	90, 90, 120	90, 90, 120
resolution (Å)[a]	32.0−2.40 (2.49−2.40)	141.4−1.85 (1.92−1.85)	34−2.2 (2.28−2.20)	142−2.3 (2.38−2.30)	78.3−3.0 (3.11−3.0)	77.6−2.2 (2.28−2.20)	77.6−2.7 (2.85−2.70)
R_{sym}[a]	11.3 (37.5)	9.1 (44.9)	10.3 (47.3)	9.1 (44.2)	10.3 (62.9)	9.4 (40.2)	9.7 (42.8)
$I/I\sigma$[a]	8.7 (2.1)	23 (2.5)	9.8 (2.2)	21.8 (2.1)	15.3 (1.9)	17.7 (2.6)	6.4 (1.8)
completeness (%)[a,b]	93.2 (79.8)	93.5 (76.0)	96.4 (91.2)	80.8 (58.9)	88.7 (66.0)	81.9 (42.7)	97.7 (98.7)
redundancy	3.1	5.4	2.5	6.0	6.3	6.3	2.4
Refinement							
resolution (Å)	32−2.4	141.4−1.8	20−2.2	42−2.5	78.3−3.0	77.6−2.2	77.6.2−2.7
no. of reflections	98363	216309	131814	81268	17705	40251	26223
R_{work}/R_{free}[a]	17.8/24.5	19.0/23.1	22.0/27.6	20.4/27.5	23.6/30.0	21.3/26.9	23.7/30.3
no. of molecules							
protein residues	1988	1988	1988	1988	780	781	781
N-acetylglucosamine (NAG)	4	4	4	6	4	12	11
mannose (MAN)						2	5
sulfate anion (SO_4^{2-})			28		1	4	5
phosphate anion (PO_4^{3-})	64	63		50			
glycerol (GOL)	5						
chaperone	2 (IFG)						2 (DGJ)
Tris						1	
galactose						2	
water	923	1699	1181	222		162	73
B-factor							
protein	26.2	26.1	24.6	49.2	121.0	71.1	63.4
NAG	34.8	33.7	30.9	62.3	139.6	93.0	80.8
MAN						199.9	88.5
SO_4^{2-}			46.7		126.9	91.0	
PO_4^{3-}	74.6	63.4		79.4			
GOL	43.9						
chaperone	28.2						58.5
Tris						58.7	
galactose						55.6	
water	29.0	37.7	28.5	43.3		54.3	45.0
rmsd							
bond lengths (Å)	0.02	0.017	0.016	0.016	0.018	0.020	0.016
bond lengths (deg)	1.957	1.683	1.682	1.706	1.844	2.049	1.912

[a] Data for the highest-resolution shell are given in parentheses; 5% of reflections were selected for R_{free}. [b] GCase crystals are shaped as thin plates that diffract anisotropically along their thin edge, resulting in incomplete data in the highest-resolution bin. α-Gal A crystals are very radiation sensitive rods, so some data were not collected in the highest-resolution bin.

emission at 460 nm), and α-Gal A or GCase activity was plotted as a function of pH.

RESULTS

Enzyme Activity Profile. The enzyme activities of α-Gal A and GCase were measured in the pH range of 4.5−8.2. Consistent with their lysosomal function, α-Gal A and GCase exhibit pH sensitive enzyme activity (Figure 1c,d). Activity profiles of GCase and α-Gal A indicate that maximal activity is observed at a lysosomal pH of < 6, and most enzyme activity is abolished at the neutral pH of the endoplasmic reticulum (pH 7.4). These results for recombinant enzymes are consistent with previous activity studies of α-Gal A (*67*) and GCase (*68*) isolated and purified from human placenta and spleen, respectively, and correlate with thermostability (see below).

Structural Comparisons. *(i) GCase*. Previously, we observed variability in the active site region of independent monomers in the asymmetric unit of apo GCase at pH 7.5 (PDB entry 2NT1) (*23*). Specifically, loop 1 was found in an α-helical conformation in two of the four crystallographic monomers in the asymmetric unit, and extended in the remaining two monomers. Because these conformations were seen in the absence of ligand, we suggested that the two conformations of loop 1 trapped crystallographically are sampled upon folding in the ER (*23*). In our previous study, we presumed that the pH 4.5 glycerol-bound (*23*) or sulfate-bound (*39*) GCase structures grown from ammonium sulfate were identical to that of apo GCase, because only one conformation, that in which loop 1 is in an extended conformation, had been observed in those structures.

To systematically examine the effects of pH and crystallization cocktail on these observed loop conformations and to address the conformational variability of the active site loops with pH and inhibitor binding, we determined the crystal structures of IFG-bound GCase at pH 7.5 (C1) cryoprotected with glycerol and apo GCase at pH 5.5 (C2) and pH 4.5 [C3 and *C*4 (Tables 1 and 2)]. All apo structures were flash-cooled in 1.8 M Li_2SO_4 and buffer, omitting glycerol and ethylene glycol that are typically used as cryoprotectants and could bind in the active site. C3 and C4 differ in the method used for crystallization. C3 was grown from ammonium sulfate and frozen with Li_2SO_4 directly, whereas C4 was obtained by taking crystals grown from phosphate salts at pH 5.5 and soaking them in a suitable solution at pH 4.5 prior to cryoprotection. A comparison of C3 and C4 therefore enables the identification of any effects of crystallization cocktail at pH 4.5. C2 and C4 bracket the reported lysosomal pH range of 4.7−5.5 (*1*).

The three apo GCase structures are nearly identical (rmsd of ~0.45 Å over all pairs of crystallographically observed monomers), each with the same two α-helical and two extended loop 1 conformations observed among the four independent monomers in the crystallographic asymmetric unit. These apo structures are also nearly indistinguishable from 2NT1. In comparison to the rest of the enzyme, the loop 1 and loop 2 regions have the highest thermal *B*-factors (Figure 2a). We observed a correlation between interpretable, yet comparatively poor, $2F_o - F_c$ electron density for the extended conformation for loop 1 paired with excellent electron density for loop 2, and vice versa. Thus, there appears to be no crystallization cocktail or pH bias for these loop conformations (Figure 2b). Given that the structures are determined to similar resolution limits, the high thermal factors of loops 1 and 2 suggest that in the low-pH environment observed in the lysosome, these loops are likely to be sampling several conformations. Thus, for the GCase polypeptide alone, the full active site, which comprises the catalytic center and hydrophobic subsites created by loops 1 and 2, does not appear to be preorganized for substrate binding. The native catalytic environment of GCase, which involves proximity to the lysosomal membrane and binding to saposin C in a poorly understood fashion (*69*), may also influence the conformation of the GCase active site.

The overall structure of IFG-bound GCase at pH 7.5 (C1) is similar to our previously determined structures of IFG-bound GCase at pH 4.5 [PDB entry 2NSX, rmsd of 0.19 Å (Figure 3a)] and of apo GCase in the α-helical conformation [PDB entry 2NT1, rmsd of 0.38 Å (Figure 3b)] (*23*). Like for 2NSX, IFG is

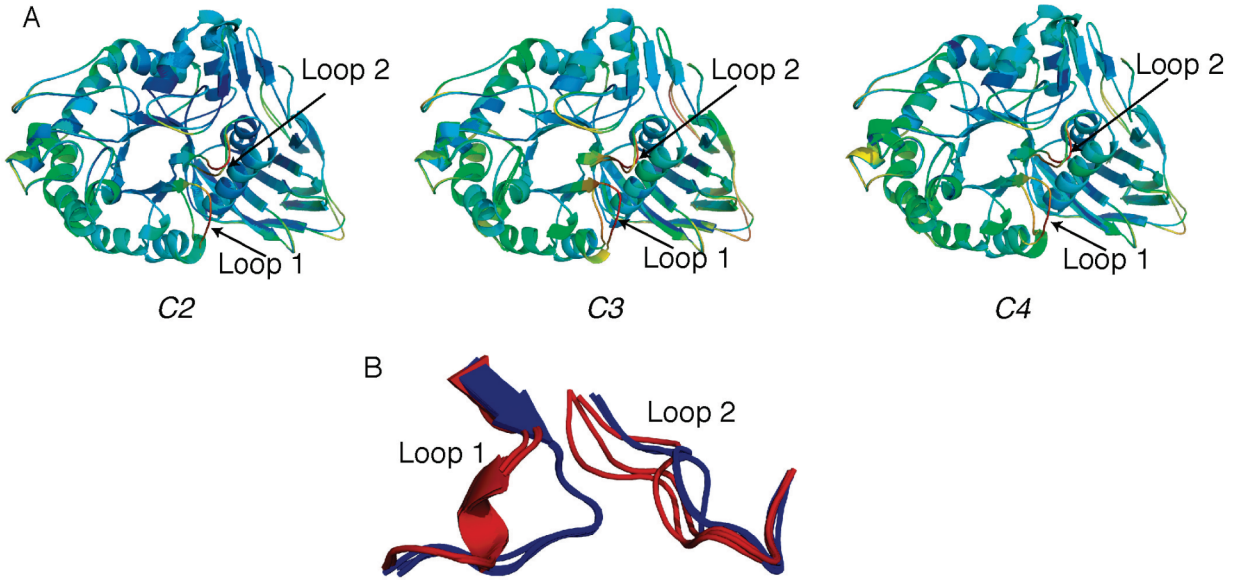

FIGURE 2: Structures of apo GCase grown under different conditions. Overlay of two monomers in the asymmetric unit exhibiting distinct loop 1 structures (α-helical or extended). (A) C2 at pH 5.5, C3 at pH 4.5, and C4 at pH 4.5 (soaked). Ribbon diagrams are colored using a rainbow corresponding to an increasing thermal factor from blue (low *B*-factor) to red (high *B*-factor). (B) Superposition of structures in panel A in the loop 1, loop 2 region. Red for α-helical loop 1 and blue for extended loop 1 conformation.

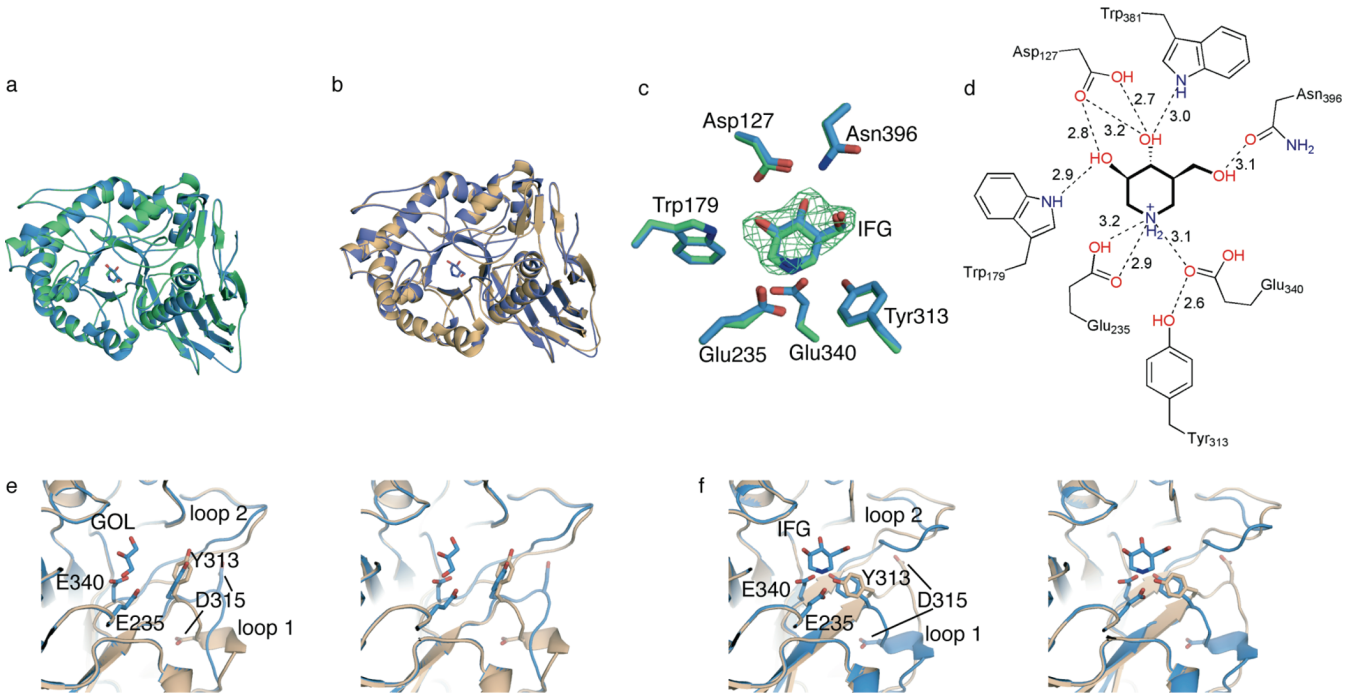

FIGURE 3: GCase structures at various pHs and in complex with IFG. (A) Overlay of the GCase structure with IFG at pH 4.5 (PDB entry 2NSX, green) and pH 7.5 (C1, this work, blue). (B) Overlay of IFG-bound C1 (blue) with with apo GCase at pH 5.5 (C2, beige) exhibiting α-helical loop 1. (C) Superposition of active site residues from the overlay shown in panel a. $F_o - F_c$ difference density from initial rigid body refinement contoured at 3σ. (D) Schematic diagram of hydrogen bonding interactions involved in stabilizing IFG in the active site of C1. Distances are in angstroms. (E) Active site stereoview of the glycerol-bound monomer of C1 superimposed with the corresponding monomer from apo form GCase at pH 7.5 (2NT1). (F) Active site stereoview of the IFG-bound monomer of C1 superimposed with the corresponding monomer from apo GCase at pH 7.5 (2NT1). For panels e and f, the bound ligand, nucleophilic (Glu 340) and basic (Glu 235) residues, and two key loop 1 residues (Tyr 313 and Asp 315) are shown in ball-and-stick representation.

bound in C1 in two of the four monomers in the asymmetric unit, and glycerol is found in the remaining two monomers. The catalytic centers of 2NSX and C1 (Figure 3c) are nearly indistinguishable: the active site residues are locked into the same conformation, and IFG is held in place by the same interacting residues at comparable distances (Figure 3d). This result suggests that the protonation states of acidic active site residues are unchanged, and it is consistent with (a) the pK_a of 8.4 for IFG (*70*) and (b) the low pK_a of the catalytic acid−base residues. Alternatively, the protonation state of IFG may not alter the structure of GCase.

Surprisingly, IFG binds to the monomers in the asymmetric unit where loop 1 is observed in the extended conformation for apo GCase (comparison here is to the apo structures C2−C4 and 2NT1), resulting in a rearrangement to the α-helical conformation, and glycerol is found in the active site of the remaining monomers where loop 1 is unwound (Figure 3e,f). Glycerol and IFG bind in the active site and appear to induce GCase into a particular conformation, but only IFG can thermally stabilize GCase (see below) and is a pharmacological chaperone. It would seem that the particular induced fit of IFG-bound GCase is the substrate-ready conformation of GCase, and this configuration is important for pharmacological chaperoning of GCase. However, given that the oligomeric state of GCase in vivo is not fully understood (*45*, *46*, *68*), further experiments will be required to rule out the possibility that GCase exists as a cooperative dimer in which the conformation of loop 1 in one monomer is coordinated with that of the second monomer. For example, IFG binding in the active site of one GCase monomer may induce the unwinding of loop 1 in the second GCase monomer, which in turn enables glycerol to bind in the active site, or vice versa. The lifetime of the conformational change induced by IFG after exchange for substrate in vivo remains an open question as well.

(ii) α-*Gal A*. To elucidate pH-dependent features of α-Gal A, we determined structures of apo (3.0 Å resolution), galactose-soaked (2.2 Å resolution), and DGJ-soaked (2.7 Å resolution) α-Gal A derived from a Chinese hamster ovary cell line (*71*) at pH 4.5. The asymmetric unit contains one α-Gal A dimer, and although we subjected our protein samples to deglycosylation with N-glycosidase F, numerous carbohydrate linkages are visible in the crystal structures. This is the first report of DGJ-bound α-Gal A, and we compared our structures with previously determined structures of fully glycosylated α-Gal A derived from a human cell line complexed with ethylene glycol and galactose at pH 7.5 (PDB entries 1R46 and 1R47, respectively) (*40*). The three-dimensional structures of α-Gal A complexed with the hydrolysis product, galactose, or the product analogue inhibitor DGJ show no polypeptide backbone or active site changes compared to apo α-Gal A (Figure 4a, rmsd for Cα atoms of ~0.4 Å), but we observe considerably higher *B*-factors for the lowest-resolution apo structure compared to DGJ- or galactose-bound α-Gal A. Similarly, the three-dimensional structure of the protein does not change as a function of pH, presumably because the disulfide bonds at the mouth of the active site and elsewhere in the protein preclude such a dramatic rearrangement. Galactose and DGJ bind in the α-Gal A active site with similar distorted chair conformations (Figure 4b,c), with the methoxy arm of DGJ (Figure 1a) stabilized through interactions with Asp 93. Extensive hydrogen bonding and electrostatic interactions are observed to stabilize these ligands in the α-Gal A active site, but the 2.7 Å resolution limit of the structure of DGJ-bound

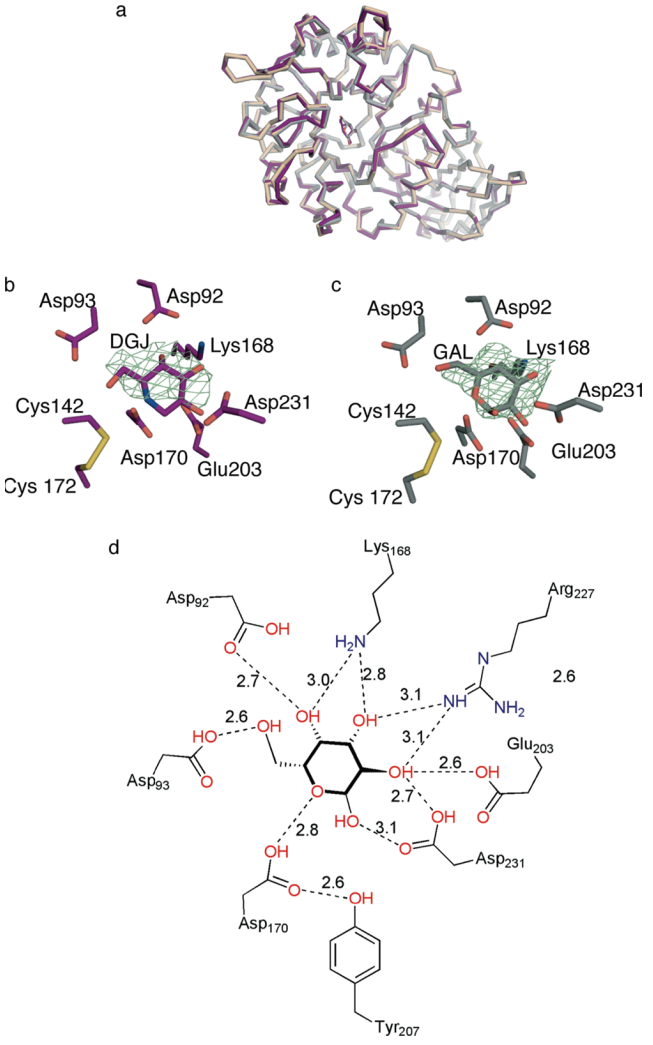

FIGURE 4: α-Gal A structures. (A) Superposition of apo α-Gal A (beige), galactose-bound α-Gal A (silver), and DGJ-bound α-Gal A (purple). (B) Active site region of DGJ-bound α-Gal A. $F_o - F_c$ difference density immediately following original molecular replacement solution contoured at 2.5σ. (C) Active site region of galactose-bound α-Gal A. $F_o - F_c$ difference density immediately following original molecular replacement solution at 3σ. (D) Schematic diagram of hydrogen bonding interactions involved in stabilizing galactose in the active site of DGJ. Distances are in angstroms.

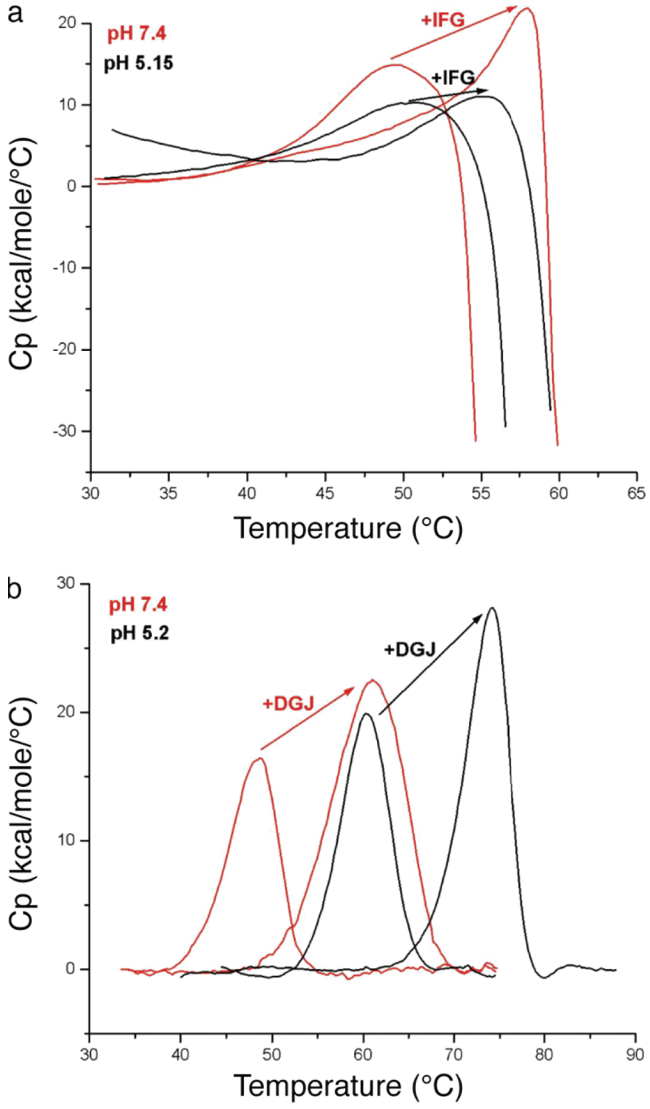

FIGURE 5: Differential scanning calorimetry. (A) Thermal denaturation of GCase upon addition of IFG at pH 7.4 (red) and 5.2 (black). (B) Thermal denaturation for α-Gal A upon addition of DGJ at pH 7.4 (red) and 5.2 (black).

α-Gal A precludes precise measurement of H-bonding distances for the chaperone. The galactose-bound structure is the only α-Gal A structure in which significant numbers of water molecules are visible, and because of its higher resolution (2.2 Å), we can report hydrogen bonding distances (Figure 4d). The higher resolution of the galactose-bound complex was enabled by the large size of the crystal. In addition, a strong peak in the difference ($F_o - F_c$) electron density map is found at the dimer interface. This peak was modeled as a Tris molecule, presumably from the protein buffer. The functional significance of a bound ligand in this interface is currently unknown but could be important for the design of pharmacological chaperones that bind to regions remote from the active site of α-Gal A and stabilize the functional dimer (see below). Notably, like IFG-bound GCase but not apo or glycerol-bound GCase, a tyrosine residue, Tyr 207, is H-bonded with a 2.6 Å distance to the α-Gal A nucleophile Asp 170. Thus, in contrast to GCase, apo α-Gal A appears preorganized for catalysis, and its apo structure likely represents the active conformation. This prearrangement is consistent with the broad range of α-galactose-containing substrates that can be hydrolyzed by α-Gal A (*72*).

Stability Comparisons. To study the stability conferred by pharmacological chaperones on GCase and α-Gal A, we used differential scanning calorimetry (DSC). We recorded denaturation thermograms for GCase and α-Gal A at pH 5.2 and 7.4 in the presence and absence of their respective pharmacological chaperones (Figure 5).

(i) GCase. GCase precipitates immediately after the folding−unfolding transition has occurred, which is observed by the heat capacity falloff in DSC (Figure 5a). Thus, we cannot extract thermodynamic parameters from these data and are limited to comparing relative melting temperatures and shapes of the melting curves. A modest increase in the melting temperature (T_m) of GCase is observed for the acidic-pH environment when compared to neutral pH [49.3 °C at pH 7.4 vs 51.7 °C at pH 5.2 (Figure 5a and Table 3A)]. A broad transition is observed for apo GCase at both pH values (Figure 5a), indicating low cooperativity and possibly a population of intermediate states during unfolding. One hypothesis for explaining this behavior is that the domains of GCase are not composed of distinct regions of the

Table 3: Summary of Melting Temperatures from Differential Scanning Calorimetry of (A) GCase with and without IFG at pH 7.4 and 5.15 and (B) α-Gal A with and without DGJ at pH 7.4 and 5.2

		T_m (°C)
	(A) GCase	
pH 7.4	GCase	49.3
	GCase with IFG	58.0
pH 5.2	GCase	51.7
	GCase with IFG	55.4
	(B) α-Gal A	
pH 7.4	α-Gal A	48.0
	α-Gal A with DGJ	60.6
pH 5.2	α-Gal A	60.2
	α-Gal A with DGJ	73.5

Table 4: Thermodynamic Parameters for Thermal Denaturation of α-Gal A with and without DGJ at pH 7.4 and 5.2

		ΔH_{cal} ($\times 10^5$ cal)	ΔH_{vH} ($\times 10^5$ cal)	χ^2 ($\times 10^6$)	fit analysis
pH 7.4	GLA	1.18	1.16	1.9	two-state
	GLA with DGJ	2.11	0.91	2.1	non-two-state
pH 5.2	GLA	1.41	1.31	0.33	two-state
	GLA with DGJ	2.12	1.32	1.47	non-two-state

amino acid chain (see above), and thus, the unfolding pathway may involve many intermediate conformational variations.

In the presence of a slight molar excess of IFG, the melting temperature of GCase measured by DSC increases reproducibly to 58 °C at pH 7.4 and to 55.4 °C at pH 5.2 (Figure 5a and Table 3A). Thus, the binding of IFG to GCase confers more stability to GCase at a neutral pH reflective of the ER than at a pH of the lysosome. Presumably, this effect is dictated by the nanomolar binding affinity of IFG (*23*). In addition, binding of IFG to GCase sharpens the folding−unfolding transition of the denaturation curves, suggesting a more cooperative unfolding transition when IFG is bound. It is likely that IFG binding to the TIM barrel of GCase reduces its conformational flexibility, leading to increased thermostability and cooperativity of unfolding.

(ii) α-*Gal A*. α-Gal A undergoes thermal unfolding without aggregation (Figure 5b), and we conducted the α-Gal A unfolding experiments under conditions of microscopic reversibility (see Experimental Procedures). The stability of apo α-Gal A exhibits considerable pH sensitivity: the T_m is 48 °C at pH 7.4 and 60.2 °C at pH 5.2 (Table 3B). Thermal unfolding of apo α-Gal A at both pH values is accompanied by an enthalpy of ~100 kcal/mol per dimer that is fit well to a two-state model (Table 4). These results suggest that dissociation of the dimer and unfolding of each monomer occur simultaneously (*73*), and hence, the folded monomer is not stable. The lack of concentration dependence on T_m further supports the model in which no dissociation of the dimer occurs prior to unfolding.

The addition of DGJ to α-Gal A at both pH values increases the T_m ~13 °C, to 60.6 °C at pH 7.4 and to 73.5 °C at pH 5.2 (Table 3B). In contrast to the case for GCase with IFG, the increase in stability of α-Gal A with DGJ bound is approximately the same at low and high pH. The calorimetric enthalpy of unfolding of α-Gal A in the presence of DGJ is ~200 kcal/mol per dimer, which corresponds to twice the calculated van't Hoff (two-state) enthalpy (Table 4). van't Hoff analysis suggests that ligand binding in this case results in a non-two-state unfolding transition with lower cooperativity. One possibility is that ligand binding leads to the preferential stabilization of the TIM barrel domain where binding takes place. Specifically, the TIM barrel, stabilized by the binding of DGJ, and β-barrel domains within each α-Gal A monomer unfold independently but at the same temperature. Two lines of evidence support this interdomain cooperativity for unfolding of α-Gal A with DGJ. First, the half-inhibitory concentration (IC_{50}) is in the nanomolar range for the inhibition of α-Gal A by DGJ (*54*), and we have shown that DGJ binds in the active site, located in the TIM barrel. With a slight excess of DGJ, all available active sites are expected to be saturated with inhibitor, and no other binding sites have been identified for DGJ on α-Gal A. Second, Sturtevant plot analysis, which uses the slope of the plot of $1/T_m$ and ln[ligand] to determine the number of bound ligands per molecule, indicates 1.7 DGJ molecules, or close to 2, are bound per dimer for α-Gal A. This analysis uses the slope of the plot of $1/T_m$ and ln[ligand] to determine the number of bound ligands per molecule. No plateau is expected in a plot of T_m versus ligand concentration if the ligand binds only to the folded state of the enzyme. This behavior is well-documented and a result of the interplay between temperature-dependent (a) equilibrium between the folded and unfolded protein conformations, (b) the binding constant of the ligand for the folded enzyme, and (c) unfolding coupled to ligand dissociation (*64*−*66*).

DISCUSSION

In the ER, numerous protein chaperones aid the folding of a nascent polypeptide, influence the timing of folding, or recognize features or flaws of the newly folded protein, such as the extent of glycosylation or disulfide bond formation (*9*, *10*, *74*). These quality control systems are highly redundant and have evolved to prevent proteins compromised in any way from continuing on the path to maturation. Primary quality control in the ER is thought to be governed by certain biophysical properties of the folded protein, namely, reduced thermal stability as detected by incorrectly exposed hydrophobic patches or mobile loops. Proteins recognized as misfolded can be refolded and recovered by the ER-assisted folding (ERAF) pathway or degraded by the ER-associated degradation (ERAD) pathway (*75*). Conditions that destabilize proteins, such as missense mutations or changes in pH, can shift the fate toward ERAD and reduce the degree of ER export. Because the newly folded protein is not tested for partial function, many mutant proteins, which exhibit properties different from those of the wild-type protein, do not have the opportunity to perform their cellular function before they are degraded. The lack of activity due to ER degradation often leads to disease states, such as those described here for Gaucher and Fabry disease.

Conversely, conditions that stabilize proteins, such as the presence of pharmacological chaperones, osmolytes, or a reduced temperature of cell growth, can increase the fraction of newly folded enzyme capable of ER export. The goal of pharmacological chaperones is to bind specifically to a partially active mutant enzyme target to pass detection by ER quality control machinery and promote proper cellular trafficking. There are several ways that a pharmacological chaperone may help trafficked proteins, both wild-type and mutant, pass the ER quality control system and reach their correct destinations. The chaperone may (1)

interact while the protein is folding and decrease the amount of time it takes to fold, thereby reducing the chance that it will be recognized as unfolded; (2) bind once the protein is fully folded and stabilize it so that it is less likely to unfold or to be recognized as misfolded; (3) stabilize the protein and promote normal post-translational modification (e.g., glycosylation) and processing within the ER lumen; (4) stabilize the protein in environments that would otherwise promote unfolding or degradation such as the low pH of the endosome and lysosome or the protease-rich environment of the lysosome; (5) induce or stabilize a conformation that promotes interaction with a binding partner required for proper trafficking; or (6) use all or some combination of the above.

For Gaucher and Fabry disease specifically, understanding the structural properties of GCase and α-Gal A in the neutral-pH environment of the ER to the lower-pH environment of the lysosome provides valuable insight. We hypothesized that DGJ and IFG promote export from the ER at least in part by stabilizing these enzymes in the neutral-pH environment of the ER. Since α-Gal A and GCase have little catalytic activity at neutral pH (Figure 1c,d), it was not clear if the active site of these enzymes was preserved. In this study, we used X-ray crystallography to explain how the structures of GCase and α-Gal A respond to pH changes and ligand binding. The organic solvents and other components of the crystallization mother liquor for GCase have no effect on the behavior of loop 1, providing further evidence that the induced conformation with IFG is functionally relevant. The α-helical conformation in loop 1 is present at low and neutral pH but unwinds in the presence of glycerol, which is known not to be an effective stabilizer even though it binds to the catalytic center. By contrast, induction of a specific conformation is not a feature of the action of DGJ as a chaperone for α-Gal A; therefore, we have shown that conformational changes are not a necessary feature of an effective chaperone. We also used differential scanning calorimetry to show that pharmacological chaperones enhance the stability of GCase and α-Gal A. Both GCase and α-Gal A are more stable at low pH where they are most active, and the addition of the respective iminosugar increases the stability of both enzymes at neutral pH. However, the stability conferred to GCase by IFG is greater at neutral pH than acidic at pH, an effect not observed for the DGJ−α-Gal A complex. Notably, although several studies have addressed GCase stability with pharmacological chaperones by circular dichroism (*28*, *30*) or fluorescence (*6*), these techniques do not provide insight into the unfolding pathway. To the best of our knowledge, this thermodynamic stability analysis is the first such study of α-Gal A. Our experiments were performed with recombinant wild-type human GCase and α-Gal A, but similar binding events and protein stabilization likely occur for missense mutant versions of these lysosomal enzymes that retain catalytic activity in vitro. We (*23*) and other researchers (*6*, *29*, *30*, *76*) have shown that small molecule inhibitors, including IFG, improve the export of GCase from the ER and increase lysosomal levels of both wild-type and mutant GCase in patient-derived cell lines. From a clinical standpoint, our results are directly applicable to dual therapy involving (wild-type) enzyme replacement therapy with pharmacological chaperones. This approach may improve the efficacy of enzyme replacement therapy by increasing the stability and lifetime of recombinant GCase in Gaucher patients.

In summary, we have shown that the biophysical properties of GCase and α-Gal A are consistent with their known function in the low-pH environment of the lysosome, and these properties may be useful for the development of new pharmacological chaperones. With the knowledge that an increase in stability, but not necessarily induction of a particular conformational change, may be key for an effective chaperone, it should now be possible to design a pharmacological chaperone remote from the active site or at a dimer interface. A remote binder would confer stability to the mutant enzyme and enable proper trafficking and would eliminate competition with the substrate for the active site once in the lysosome. High-throughput screening has identified compounds that enhance GCase activity yet are unlikely to bind in the active site (*77*). The binding sites for these compounds are not known, but some non-active site hot spots for ligand binding on GCase have been identified recently experimentally and by in silico methods (*78*). Lastly, it is not known whether α-Gal A dimerizes or interacts with other proteins to facilitate export from the ER. Although crystallographic studies did not reveal a change in α-Gal A conformation upon binding of DGJ, complex folding pathways are known for dimeric proteins (*79*). For GCase, new evidence implicates the lysosomal integral membrane II (LIMP-2) as its lysosomal trafficking partner (*72*), although this trafficking mechanism may be tissue-specific (*80*). Successful export of GCase from the ER is likely conditional on the binding of LIMP-2 to GCase, which may depend on the specific conformation of GCase and its stability. We are currently investigating these possibilities.

ACKNOWLEDGMENT

We are grateful to Amicus Therapeutics for IFG and DGJ, conducting the activity assays (John J. Flanagan), and valuable discussions and critical review of the manuscript (Brandon Wustman, David Lockhart, and Hung Do). We are grateful to Debby Pheasant at the Biophysical Instrumentation Facility for the Study of Complex Macromolecular Systems at MIT for calorimetric measurements.

REFERENCES

1. Anderson, R. G., and Orci, L. (1988) A view of acidic intracellular compartments. *J. Cell Biol. 106*, 539–543.
2. Futerman, A. H., and van Meer, G. (2004) The cell biology of lysosomal storage disorders. *Nat. Rev. Mol. Cell Biol. 5*, 554–565.
3. Sawkar, A. R., D'Haeze, W., and Kelly, J. W. (2006) Therapeutic strategies to ameliorate lysosomal storage disorders: A focus on Gaucher disease. *Cell. Mol. Life Sci. 63*, 1179–1192.
4. Grace, M. E., Newman, K. M., Scheinker, V., Berg-Fussman, A., and Grabowski, G. A. (1994) Analysis of human acid β-glucosidase by site-directed mutagenesis and heterologous expression. *J. Biol. Chem. 269*, 2283–2291.
5. Liou, B., Kazimierczuk, A., Zhang, M., Scott, C. R., Hegde, R. S., and Grabowski, G. A. (2006) Analyses of variant acid β-glucosidases: Effects of Gaucher disease mutations. *J. Biol. Chem. 281*, 4242–4253.
6. Kornhaber, G. J., Tropak, M. B., Maegawa, G. H., Tuske, S. J., Coales, S. J., Mahuran, D. J., and Hamuro, Y. (2008) Isofagomine induced stabilization of glucocerebrosidase. *ChemBioChem 9*, 2643–2649.
7. Steet, R. A., Chung, S., Wustman, B., Powe, A., Do, H., and Kornfeld, S. A. (2006) The iminosugar isofagomine increases the activity of N370S mutant acid β-glucosidase in Gaucher fibroblasts by several mechanisms. *Proc. Natl. Acad. Sci. U.S.A. 103*, 13813–13818.
8. Ron, I., and Horowitz, M. (2005) ER retention and degradation as the molecular basis underlying Gaucher disease heterogeneity. *Hum. Mol. Genet. 14*, 2387–2398.
9. Ellgaard, L., and Helenius, A. (2003) Quality control in the endoplasmic reticulum. *Nat. Rev. Mol. Cell Biol. 4*, 181–191.
10. Ellgaard, L., Molinari, M., and Helenius, A. (1999) Setting the standards: Quality control in the secretory pathway. *Science 286*, 1882–1888.
11. Barton, N. W., Brady, R. O., Dambrosia, J. M., Di Bisceglie, A. M., Doppelt, S. H., Hill, S. C., Mankin, H. J., Murray, G. J., Parker, R. I.,

and Argoff, C. E.; et al. (1991) Replacement therapy for inherited enzyme deficiency: Macrophage-targeted glucocerebrosidase for Gaucher's disease. *N. Engl. J. Med. 324*, 1464–1470.
12. Zarate, Y. A., and Hopkin, R. J. (2008) Fabry's disease. *Lancet 372*, 1427–1435.
13. Elstein, D., Hollak, C., Aerts, J. M., van Weely, S., Maas, M., Cox, T. M., Lachmann, R. H., Hrebicek, M., Platt, F. M., Butters, T. D., Dwek, R. A., and Zimran, A. (2004) Sustained therapeutic effects of oral miglustat (Zavesca, N-butyldeoxynojirimycin, OGT 918) in type I Gaucher disease. *J. Inherit. Metab. Dis. 27*, 757–766.
14. Pastores, G. M., Barnett, N. L., and Kolodny, E. H. (2005) An open-label, noncomparative study of miglustat in type I Gaucher disease: Efficacy and tolerability over 24 months of treatment. *Clin. Ther. 27*, 1215–1227.
15. Allen, M. J., Myer, B. J., Khokher, A. M., Rushton, N., and Cox, T. M. (1997) Pro-inflammatory cytokines and the pathogenesis of Gaucher's disease: Increased release of interleukin-6 and interleukin-10. *Q. J. Med. 90*, 19–25.
16. Fan, J. Q., and Ishii, S. (2007) Active-site-specific chaperone therapy for Fabry disease. *FEBS J. 274*, 4962–4971.
17. Kolter, T., and Wendeler, M. (2003) Chemical chaperones: A new concept in drug research. *ChemBioChem 4*, 260–264.
18. Yu, Z., Sawkar, A. R., and Kelly, J. W. (2007) Pharmacologic chaperoning as a strategy to treat Gaucher disease. *FEBS J. 274*, 4944–4950.
19. Yam, G. H., Bosshard, N., Zuber, C., Steinmann, B., and Roth, J. (2006) Pharmacological chaperone corrects lysosomal storage in Fabry disease caused by trafficking-incompetent variants. *Am. J. Physiol. 290*, C1076–C1082.
20. Ulloa-Aguirre, A., Janovick, J. A., Brothers, S. P., and Conn, P. M. (2004) Pharmacologic rescue of conformationally-defective proteins: Implications for the treatment of human disease. *Traffic 5*, 821–837.
21. Compain, P., Martin, O. R., Boucheron, C., Godin, G., Yu, L., Ikeda, K., and Asano, N. (2006) Design and synthesis of highly potent and selective pharmacological chaperones for the treatment of Gaucher's disease. *ChemBioChem 7*, 1356–1359.
22. Ishii, S., Chang, H. H., Kawasaki, K., Yasuda, K., Wu, H. L., Garman, S. C., and Fan, J. Q. (2007) Mutant α-galactosidase A enzymes identified in Fabry disease patients with residual enzyme activity: Biochemical characterization and restoration of normal intracellular processing by 1-deoxygalactonojirimycin. *Biochem. J. 406*, 285–295.
23. Lieberman, R. L., Wustman, B. A., Huertas, P., Powe, A. C.Jr., Pine, C. W., Khanna, R., Schlossmacher, M. G., Ringe, D., and Petsko, G. A. (2007) Structure of acid β-glucosidase with pharmacological chaperone provides insight into Gaucher disease. *Nat. Chem. Biol. 3*, 101–107.
24. Lin, H., Sugimoto, Y., Ohsaki, Y., Ninomiya, H., Oka, A., Taniguchi, M., Ida, H., Eto, Y., Ogawa, S., Matsuzaki, Y., Sawa, M., Inoue, T., Higaki, K., Nanba, E., Ohno, K., and Suzuki, Y. (2004) N-Octyl-β-valienamine up-regulates activity of F213I mutant β-glucosidase in cultured cells: A potential chemical chaperone therapy for Gaucher disease. *Biochim. Biophys. Acta 1689*, 219–228.
25. Maegawa, G. H., Tropak, M., Buttner, J., Stockley, T., Kok, F., Clarke, J. T., and Mahuran, D. J. (2007) Pyrimethamine as a potential pharmacological chaperone for late-onset forms of GM2 gangliosidosis. *J. Biol. Chem. 282*, 9150–9161.
26. Okumiya, T., Kroos, M. A., Vliet, L. V., Takeuchi, H., Van der Ploeg, A. T., and Reuser, A. J. (2007) Chemical chaperones improve transport and enhance stability of mutant α-glucosidases in glycogen storage disease type II. *Mol. Genet. Metab. 90*, 49–57.
27. Parenti, G., Zuppaldi, A., Gabriela Pittis, M., Rosaria Tuzzi, M., Annunziata, I., Meroni, G., Porto, C., Donaudy, F., Rossi, B., Rossi, M., Filocamo, M., Donati, A., Bembi, B., Ballabio, A., and Andria, G. (2007) Pharmacological enhancement of mutated α-glucosidase activity in fibroblasts from patients with Pompe disease. *Mol. Ther. 15*, 508–514.
28. Sawkar, A. R., Adamski-Werner, S. L., Cheng, W. C., Wong, C. H., Beutler, E., Zimmer, K. P., and Kelly, J. W. (2005) Gaucher disease-associated glucocerebrosidases show mutation-dependent chemical chaperoning profiles. *Chem. Biol. 12*, 1235–1244.
29. Sawkar, A. R., Cheng, W. C., Beutler, E., Wong, C. H., Balch, W. E., and Kelly, J. W. (2002) Chemical chaperones increase the cellular activity of N370S β-glucosidase: A therapeutic strategy for Gaucher disease. *Proc. Natl. Acad. Sci. U.S.A. 99*, 15428–15433.
30. Sawkar, A. R., Schmitz, M., Zimmer, K. P., Reczek, D., Edmunds, T., Balch, W. E., and Kelly, J. W. (2006) Chemical chaperones and permissive temperatures alter localization of Gaucher disease associated glucocerebrosidase variants. *ACS Chem. Biol. 1*, 235–251.
31. Tropak, M. B., Blanchard, J. E., Withers, S. G., Brown, E. D., and Mahuran, D. (2007) High-throughput screening for human lysosomal β-N-acetyl hexosaminidase inhibitors acting as pharmacological chaperones. *Chem. Biol. 14*, 153–164.
32. Tropak, M. B., Reid, S. P., Guiral, M., Withers, S. G., and Mahuran, D. (2004) Pharmacological enhancement of β-hexosaminidase activity in fibroblasts from adult Tay-Sachs and Sandhoff patients. *J. Biol. Chem. 279*, 13478–13487.
33. Yu, L., Ikeda, K., Kato, A., Adachi, I., Godin, G., Compain, P., Martin, O., and Asano, N. (2006) α-1-C-Octyl-1-deoxynojirimycin as a pharmacological chaperone for Gaucher disease. *Bioorg. Med. Chem. 14*, 7736–7744.
34. Fan, J. Q. (2003) A contradictory treatment for lysosomal storage disorders: Inhibitors enhance mutant enzyme activity. *Trends Pharmacol. Sci. 24*, 355–360.
35. Jonsson, L. M., Murray, G. J., Sorrell, S. H., Strijland, A., Aerts, J. F., Ginns, E. I., Barranger, J. A., Tager, J. M., and Schram, A. W. (1987) Biosynthesis and maturation of glucocerebrosidase in Gaucher fibroblasts. *Eur. J. Biochem. 164*, 171–179.
36. Butters, T. D. (2007) Gaucher disease. *Curr. Opin. Chem. Biol. 11*, 412–418.
37. Beutler, E., and Gelbart, T. (1996) Glucocerebrosidase (Gaucher disease). *Hum. Mutat. 8*, 207–213.
38. Cantarel, B. L., Coutinho, P. M., Rancurel, C., Bernard, T., Lombard, V., and Henrissat, B. (2009) The Carbohydrate-Active EnZymes database (CAZy): An Expert Resource for Glycogenomics. *Nucleic Acids Res. 37*, D233–D238.
39. Dvir, H., Harel, M., McCarthy, A. A., Toker, L., Silman, I., Futerman, A. H., and Sussman, J. L. (2003) X-ray structure of human acid-β-glucosidase, the defective enzyme in Gaucher disease. *EMBO Rep. 4*, 704–709.
40. Garman, S. C., and Garboczi, D. N. (2004) The molecular defect leading to Fabry disease: Structure of human α-galactosidase. *J. Mol. Biol. 337*, 319–335.
41. Dean, K. J., and Sweeley, C. C. (1979) Studies on human liver α-galactosidase. II. Purification and enzymatic properties of α-galactosidase B (α-N-acetylgalactosaminidase). *J. Biol. Chem. 254*, 10001–10005.
42. Dean, K. J., and Sweeley, C. C. (1979) Studies on human liver α-galactosidases. I. Purification of α-galactosidase A and its enzymatic properties with glycolipid and oligosaccharide substrates. *J. Biol. Chem. 254*, 9994–10000.
43. Bishop, D. F., and Desnick, R. J. (1981) Affinity purification of α-galactosidase A from human spleen, placenta, and plasma with elimination of pyrogen contamination. Properties of the purified splenic enzyme compared to other forms. *J. Biol. Chem. 256*, 1307–1316.
44. Mayes, J. S., and Beutler, E. (1977) α-Galactosidase A from human placenta. Stability and subunit size. *Biochim. Biophys. Acta 484*, 408–416.
45. Choy, F. Y., Woo, M., and Potier, M. (1986) In situ radiation-inactivation size of fibroblast membrane-bound acid β-glucosidase in Gaucher type 1, type 2 and type 3 disease. *Biochim. Biophys. Acta 870*, 76–81.
46. Dawson, G., and Ellory, J. C. (1985) Functional lysosomal hydrolase size as determined by radiation inactivation analysis. *Biochem. J. 226*, 283–288.
47. Maret, A., Potier, M., Salvayre, R., and Douste-Blazy, L. (1983) Modification of subunit interaction in membrane-bound acid β-glucosidase from Gaucher disease. *FEBS Lett. 160*, 93–97.
48. Hart, D. O., He, S., Chany, C. J.II, Withers, S. G., Sims, P. F., Sinnott, M. L., and Brumer, H.III (2000) Identification of Asp-130 as the catalytic nucleophile in the main α-galactosidase from *Phanerochaete chrysosporium*, a family 27 glycosyl hydrolase. *Biochemistry 39*, 9826–9836.
49. Premkumar, L., Sawkar, A. R., Boldin-Adamsky, S., Toker, L., Silman, I., Kelly, J. W., Futerman, A. H., and Sussman, J. L. (2005) X-ray structure of human acid-β-glucosidase covalently bound to conduritol-B-epoxide. Implications for Gaucher disease. *J. Biol. Chem. 280*, 23815–23819.
50. Sandhoff, K., and Kolter, T. (1996) Topology of glycosphingolipid degradation. *Trends Cell Biol. 6*, 98–103.
51. de Alba, E., Weiler, S., and Tjandra, N. (2003) Solution structure of human saposin C: pH-dependent interaction with phospholipid vesicles. *Biochemistry 42*, 14729–14740.
52. Ho, M. W., and O'Brien, J. S. (1971) Gaucher's disease: Deficiency of 'acid'-glucosidase and reconstitution of enzyme activity in vitro. *Proc. Natl. Acad. Sci. U.S.A. 68*, 2810–2813.
53. Yam, G. H., Zuber, C., and Roth, J. (2005) A synthetic chaperone corrects the trafficking defect and disease phenotype in a protein misfolding disorder. *FASEB J. 19*, 12–18.

54. Fan, J. Q., Ishii, S., Asano, N., and Suzuki, Y. (1999) Accelerated transport and maturation of lysosomal α-galactosidase A in Fabry lymphoblasts by an enzyme inhibitor. *Nat. Med. 5*, 112–115.
55. Asano, N., Ishii, S., Kizu, H., Ikeda, K., Yasuda, K., Kato, A., Martin, O. R., and Fan, J. Q. (2000) In vitro inhibition and intracellular enhancement of lysosomal α-galactosidase A activity in Fabry lymphoblasts by 1-deoxygalactonojirimycin and its derivatives. *Eur. J. Biochem. 267*, 4179–4186.
56. Brumshtein, B., Wormald, M. R., Silman, I., Futerman, A. H., and Sussman, J. L. (2006) Structural comparison of differently glycosylated forms of acid-β-glucosidase, the defective enzyme in Gaucher disease. *Acta Crystallogr. D62*, 1458–1465.
57. Kabsch, W. (1993) Automatic processing of rotation diffraction data from crystals of initially unknown symmetry and cell constants. *J. Appl. Crystallogr. 26*, 795–800.
58. Otwinowski, Z., and Minor, W. (1997) Processing of X-ray diffraction data collected in oscillation mode. *Methods Enzymol. 276*, 307–326.
59. Collaborative Computational Project Number 4 (1994) *Acta Crystallogr. D50*, 760–763.
60. Emsley, P., and Cowtan, K. (2004) Coot: Model-building tools for molecular graphics. *Acta Crystallogr. D60*, 2126–2132.
61. Schuttelkopf, A. W., and van Aalten, D. M. (2004) PRODRG: A tool for high-throughput crystallography of protein-ligand complexes. *Acta Crystallogr. D60*, 1355–1363.
62. Krissinel, E., and Henrick, K. (2004) Secondary-structure matching (SSM), a new tool for fast protein structure alignment in three dimensions. *Acta Crystallogr. D60*, 2256–2268.
63. Freire, E. (1995) Thermal denaturation methods in the study of protein folding. *Methods Enzymol. 259*, 144–168.
64. Sanchez-Ruiz, J. M. (2007) Ligand effects on protein thermodynamic stability. *Biophys. Chem. 126*, 43–49.
65. Fukada, H., Sturtevant, J. M., and Quiocho, F. A. (1983) Thermodynamics of the binding of L-arabinose and of D-galactose to the L-arabinose-binding protein of *Escherichia coli*. *J. Biol. Chem. 258*, 13193–13198.
66. Manly, S. P., Matthews, K. S., and Sturtevant, J. M. (1985) Thermal denaturation of the core protein of lac repressor. *Biochemistry 24*, 3842–3846.
67. Beutler, E., and Kuhl, W. (1972) Purification and properties of human α-galactosidases. *J. Biol. Chem. 247*, 7195–7200.
68. Maret, A., Salvayre, R., Negre, A., and Douste-Blazy, L. (1981) Properties of the molecular forms of β-glucosidase and β-glucocerebrosidase from normal human and Gaucher disease spleen. *Eur. J. Biochem. 115*, 455–461.
69. Alattia, J. R., Shaw, J. E., Yip, C. M., and Prive, G. G. (2007) Molecular imaging of membrane interfaces reveals mode of β-glucosidase activation by saposin C. *Proc. Natl. Acad. Sci. U.S.A. 104*, 17394–17399.
70. Jensen, H. H., Lyngbye, L., and Bols, M. (2001) A Free-Energy Relationship between the Rate of Acidic Hydrolysis of Glycosides and the pK_a of Isofagomines. *Angew. Chem., Int. Ed. 40*, 3447–3449.
71. Eng, C. M., Guffon, N., Wilcox, W. R., Germain, D. P., Lee, P., Waldek, S., Caplan, L., Linthorst, G. E., and Desnick, R. J. (2001) Safety and efficacy of recombinant human α-galactosidase A: Replacement therapy in Fabry's disease. *N. Engl. J. Med. 345*, 9–16.
72. Garman, S. C. (2006) Structural studies on a-GAL and a-GALAL: The atomic basis of Fabry and Schindler diseases. *Biocatal. Biotransform. 24*, 129–136.
73. Ragone, R. (2000) How the protein concentration affects unfolding curves of oligomers. *Biopolymers 53*, 221–225.
74. van Anken, E., and Braakman, I. (2005) Versatility of the endoplasmic reticulum protein folding factory. *Crit. Rev. Biochem. Mol. Biol. 40*, 191–228.
75. Wiseman, R. L., Powers, E. T., Buxbaum, J. N., Kelly, J. W., and Balch, W. E. (2007) An adaptable standard for protein export from the endoplasmic reticulum. *Cell 131*, 809–821.
76. Street, T. O., Bolen, D. W., and Rose, G. D. (2006) A molecular mechanism for osmolyte-induced protein stability. *Proc. Natl. Acad. Sci. U.S.A. 103*, 13997–14002.
77. Zheng, W., Padia, J., Urban, D. J., Jadhav, A., Goker-Alpan, O., Simeonov, A., Goldin, E., Auld, D., LaMarca, M. E., Inglese, J., Austin, C. P., and Sidransky, E. (2007) Three classes of glucocerebrosidase inhibitors identified by quantitative high-throughput screening are chaperone leads for Gaucher disease. *Proc. Natl. Acad. Sci. U.S.A. 104*, 13192–13197.
78. Landon, M. R., Lieberman, R. L., Hoang, Q. Q., Kozakov, D., Ju, S., Orwig, S. D., Brenke, R., Chuang, G.-Y., Beglov, D., Vajda, S., Petsko, G. A., and Ringe, D. (2009) Detection of non-catalytic binding hot spots on protein surfaces via fragment-based methods: Application of targets of neurological disorders. *J. Comput.-Aided Mol. Des.* (in press).
79. Rumfeldt, J. A., Galvagnion, C., Vassall, K. A., and Meiering, E. M. (2008) Conformational stability and folding mechanisms of dimeric proteins. *Prog. Biophys. Mol. Biol. 98*, 61–84.
80. Balreira, A., Gaspar, P., Caiola, D., Chaves, J., Beirao, I., Lima, J. L., Azevedo, J. E., and Miranda, M. C. (2008) A nonsense mutation in the LIMP-2 gene associated with progressive myoclonic epilepsy and nephrotic syndrome. *Hum. Mol. Genet. 17*, 2238–2243.